Pol J Med Phys Eng. 2008;14(3):163-182.
PL ISSN 1425-4689
doi: 10.2478/v10013-008-0014-0
website: http://www.pjmpe.waw.pl

M. Zarza Moreno[1, 2], N. Teixeira[3, 4], A. P. Jesus[1, 2], G. Mora[1]

Assesing multileaf collimator effect on the build-up region using Monte Carlo method

[1]Centro de Fisica Nuclear da Universidade de Lisboa, Lisboa, Portugal
[2]Faculdade de Ciencias e Tecnologia da Universidade Nova de Lisboa, Portugal
[3]Escola Superior de Tecnologia da Saude de Lisboa, Lisboa, Portugal
[4]Faculdade de Ciencias Medicas/Universidade Nova de Lisboa, Portugal
e-mail: miriam@cii.fc.ul.pt

Previous Monte Carlo studies have investigated the multileaf collimator (MLC) contribution to the build-up region for fields in which the MLC leaves were fully blocking the openings defined by the collimation jaws. In the present work, we investigate the same effect but for symmetric and asymmetric MLC defined field sizes (2×2, 4×4, 10×10 and 3×7 cm^2). A Varian 2100C/D accelerator with 120-leaf MLC is accurately modeled for a 6 MV photon beam using the BEAMnrc/EGSnrc code.

Our results indicate that particles scattered from accelerator head and MLC are responsible for the increase of about 7% on the surface dose when comparing 2×2 and 10×10 cm^2 fields. We found that the MLC contribution to the total build-up dose is about 2% for the 2×2 cm^2 field and less than 1% for the largest fields.

Key words: surface dose, build-up dose, MLC, IMRT, Monte Carlo.

Introduction

For several years, multileaf collimators (MLCs) have been used for 3D conformal radiotherapy (3D-CRT). Recently, with the advances in computer and linac technologies, MLCs have become a powerful tool to improve dose distribution in complex cases, for example to deliver optimized intensity-modulated dose distributions (IMRT) in static mode (SMLC or step and shoot mode) or dynamic mode (DMLC or sliding windows, and intensity-modulated arc therapy (IMAT)).

There are several studies [1–3] about specific characteristics of multiple MLC designs, in which dosimetric, geometric, and clinical aspects are analyzed using the Monte Carlo method. It has been indicated that transmission through the MLC, leaftip transmission, leaf scatter radiation and the tongue-and-groove effect can contribute to the total dose, as well as, to the surface and build-up dose. However, there is a lack of quantitative information about the overall MLC effect on the surface dose.

Previous authors [3] have investigated the MLC contribution to the build-up region. They found that the electrons ejected from the MLC contribute about 18% of the surface dose for a 6 MV beam. Monte Carlo (MC) calculations, however, were performed only for a 10×10 cm^2 MLC blocked field, and the surface dose was obtained by extrapolation of the dose to the surface.

In the present work we investigate the effect of the MLC on the build-up region dose using a detailed MC model of the MLC for symmetric and asymmetric MLC defined field sizes of 2×2, 4×4, 10×10 and 3×7 cm^2. The surface dose was calculated directly in the voxel. The contributions from the MLC contaminant particles are determined. The fluence and energy spectra of particles reaching the phantom surface are presented. The contribution of particles scattered from the MLC to total fluence is also determined.

Material and methods

A Varian 2100C/D linear accelerator with 120-leaf Millenium MLC was accurately modeled for 6 MV photon beam using the BEAMnrc/EGSnrc user code [5]. Figure 1 shows details of the treatment head configuration used in this study. The model consists of several components such as the target, primary collimator, vacuum exit window, flattening filter, monitor chamber, collimating jaws, MLC and phantom. The detailed geometry of each component of the linear accelerator was provided by the manufacturer.

A parallel circular electron beam hitting on the target with 6.2 MeV energy and a radius of 0.15 cm was chosen to match the calculated depth dose and off-axis profiles with measured data within 1–2%. The BEAMnrc component module DYNVMLC [1] was used to fully model the geometry of the MLC. The MLC model was previously validated by comparing simulated MLC leakage profiles and dose distributions for various MLC patterns with measurements.

The Monte Carlo simulations were split into three stages. First, we obtained a phase-space file at a plane after the flattening filter and before the jaws. The phase space

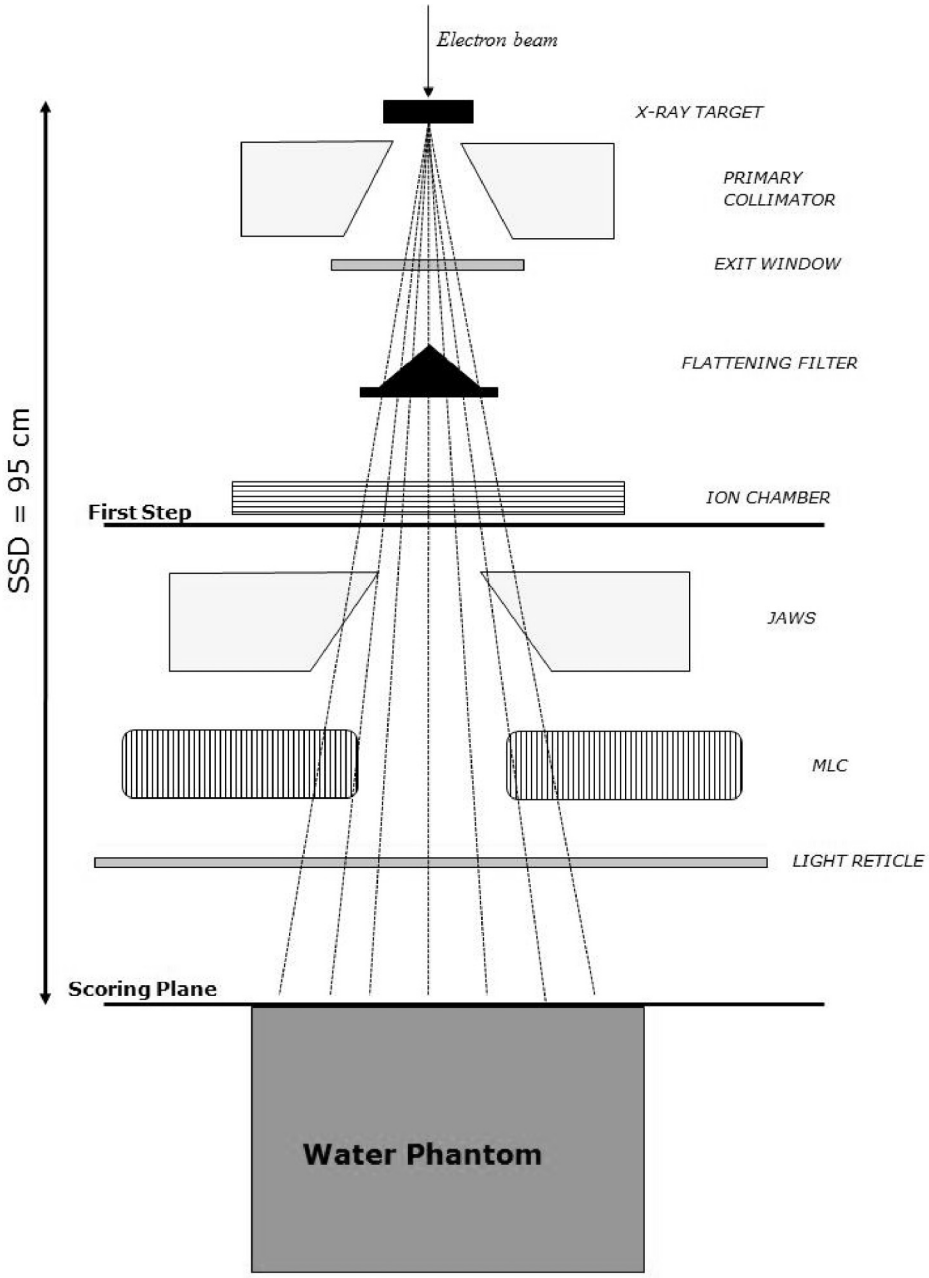

Figure 1. Schematic representation of simulated geometry of Varian 2100C/D linac head and water phantom configurations used in this study

file obtained in this way was independent of field size and was subsequently used for the next step of simulation. In the second stage, a set of output phase space files for the various MLC and JAWS field size configurations, containing the energy, position, direction, charge and history for every particle reaching the scoring plane, were obtained just above the phantom surface located at a source to surface distance (SSD) of 95 cm. Finally, these phase-space files were then used as a source in the DOSXYZnrc [6] water phantom simulations.

For the study, MLC symmetric openings of 2×2, 4×4 and 10×10 cm^2 and asymmetric 3×7 cm^2 field were simulated. For all these openings, the collimating jaws were set to back up the leaf positions by 5 mm in X and Y direction, defining 3×3, 5×5 and 11×11 cm^2 and 4×8 cm^2 fields, respectively. For the purpose of this study, we name each of these configurations 'MLC defined field'. In order to analyze the contribution of the MLC, it was useful to define a field in which the MLC leaves were withdrawn beneath the jaws so as to not intercept the beam (50×50 cm^2 MLC opening). The field size was then defined by the above mentioned collimating jaws opening. For this study, we name each of these configurations 'MLC open field'.

The dose calculations were performed for a water phantom of 20 cm radius and 3 cm thick, with a central axis scoring region of radius *r*, as shown in Figure 2. Voxels 0.025 cm were set up at shallow phantom depths (from 0 to 0.4 cm depth). Larger voxels of 0.05 and 0.1 cm thickness were used along the remaining phantom [4]. The radius *r* was set to 1 cm for the 10×10 cm^2 field and 0.5 cm for the 4×4 cm^2, 2×2 cm^2 and 3×7 cm^2 field sizes.

To avoid underestimating the surface dose, the electron cutoff energy (ECUT) and the photon cutoff energy (PCUT) for the two latter simulation stages were set to 0.521 MeV and 0.01 MeV, respectively. However, auxiliary calculations with ECUT equal to 0.700 MeV and PCUT equal to 0.01 MeV were performed in order to analyze the influence of this parameter on the results.

To improve the calculation efficiency, various variance reduction techniques, such as uniform bremsstrahlung splitting with a photon split of 20 [5] and range rejection with ESAVE of 1 MeV were employed for the first two steps of the accelerator simulation. This technique introduces one approximation by ignoring the possibility that the electron produces a photon which could then escape from the current region. Auxiliary calculations without including this approximation were done and we did not verify any effect in the calculated photon and electron spectra.

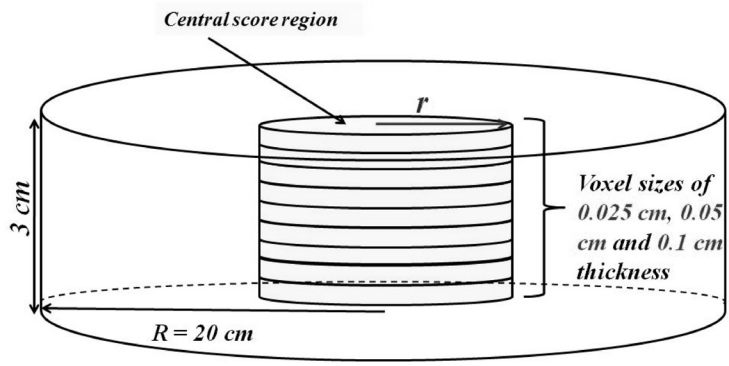

Figure 2. Simulated water phantom geometry. Voxels of 0.025, 0.05 and 0.1 cm were set up from 0 to 3 cm depth. (This figure is not to scale)

For all dose calculations, sufficient histories were run to ensure that the error for each voxel in the central axis scoring region was 1% (1σ) at depth of dose maximum (~1.5 cm), *dmax*.

Results

MLC dose contribution to total dose as function of field size

In this section, we investigate the influence of the MLC on the dose build-up curve in a homogeneous water phantom. Figures 3a–3f and 4a–4b present the comparison of relative central-axis depth dose curves for several MLC defined field sizes (10×10, 4×4, 2×2 and 3×7 cm^2) to the MLC open field respective ones. For each situation, the curves were normalized to the dose at the depth of dose maximum for the MLC open field configuration.

The effects of the MLC on the dose build-up curves are clearly seen from the differences between the dose values calculated for the MLC defined field (black solid line) and those values calculated for the MLC open field (black dashed line) for all the fields studied.

In Figures 3a–3d, it can be seen that the contribution to the dose of the MLC (10×10 and 4×4 cm^2 MLC defined fields) is very small, as differences between MLC defined field and MLC open field curves are less than 1%. For the smallest field size (2×2 cm^2), the MLC contributes about 2% of the total dose at a depth larger than 7 mm.

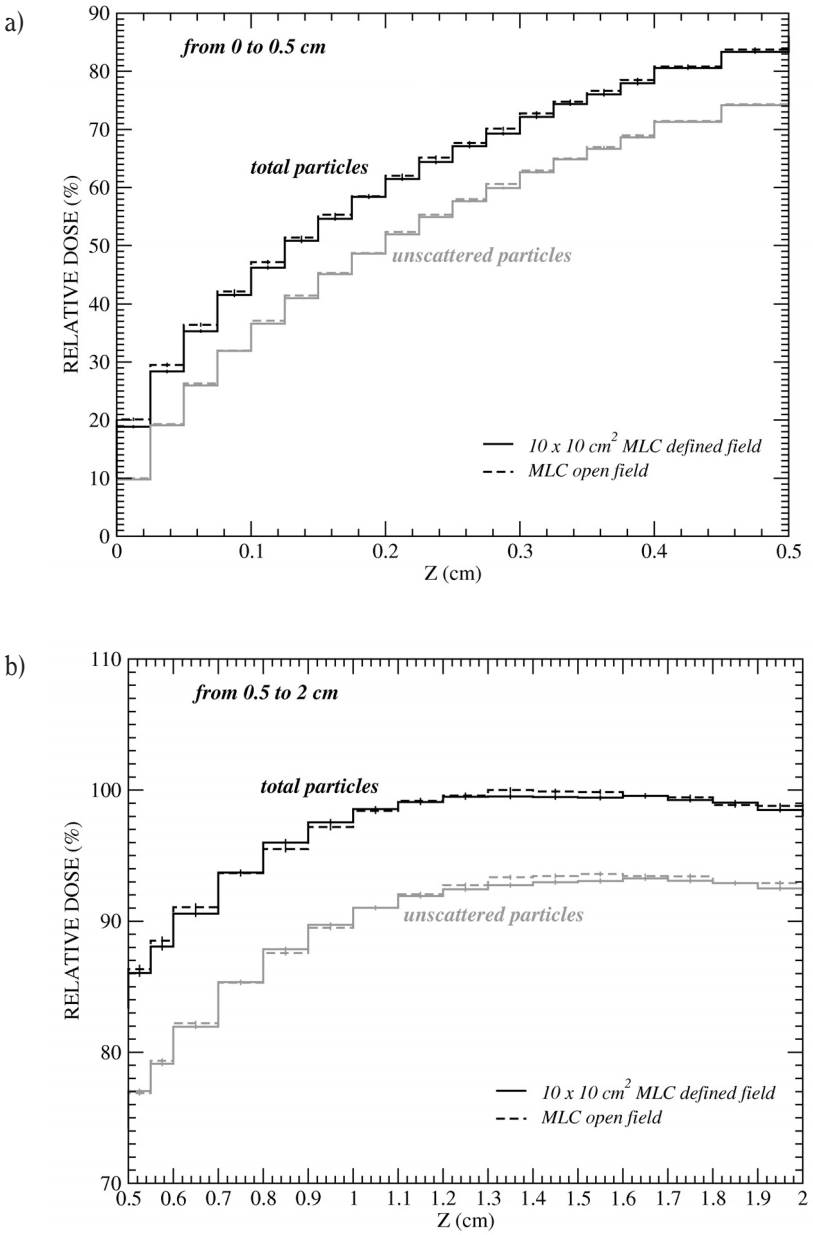

Figure 3a-b. Build-up depth dose curves for the MLC defined field size of 10×10 cm^2 in comparison to the MLC open field respective ones (dashed line). The components of the dose due to unscattered particles are shown (grey line). The curves were normalized to the D_{max} of the total dose curve for the MLC open field

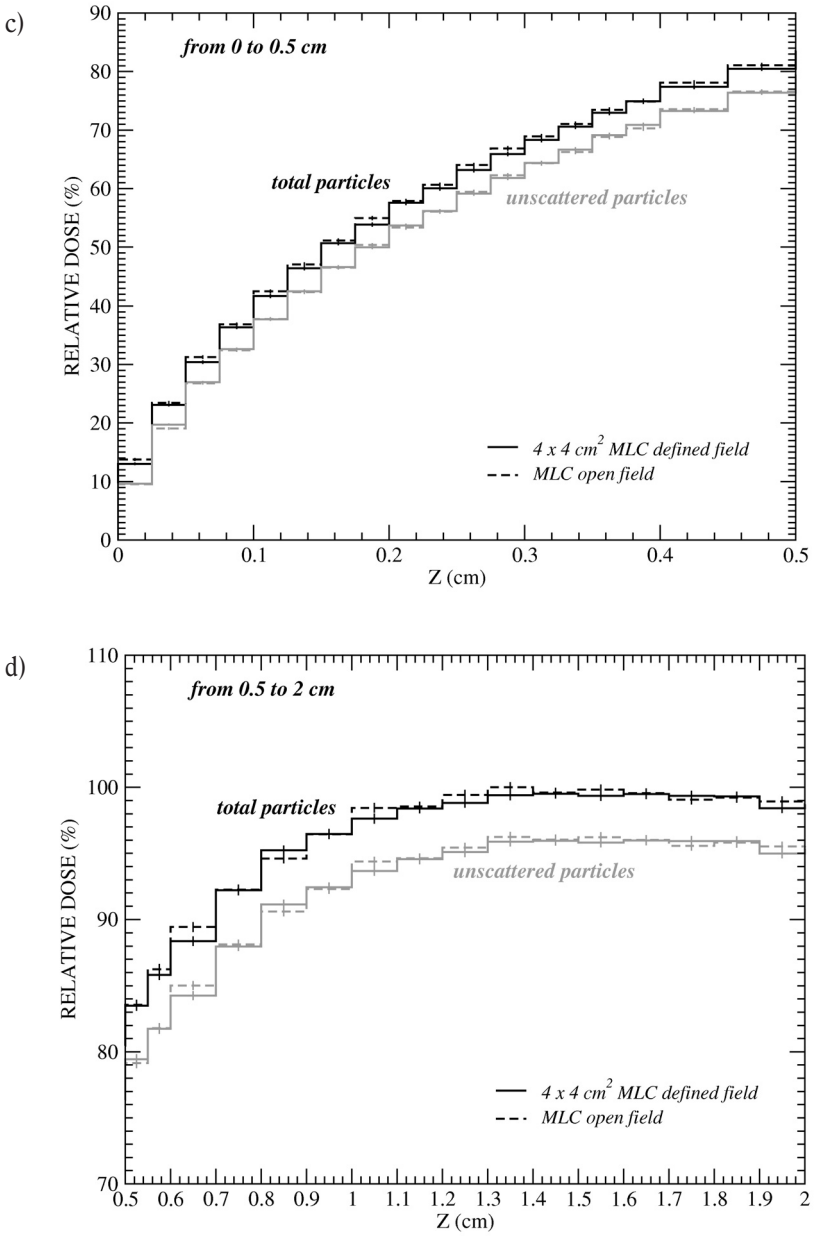

Figure 3c-d. Build-up depth dose curves for the MLC defined field size of 4×4 cm^2 in comparison to the MLC open field respective ones (dashed line). The components of the dose due to unscattered particles are shown (grey line). The curves were normalized to the D_{max} of the total dose curve for the MLC open field

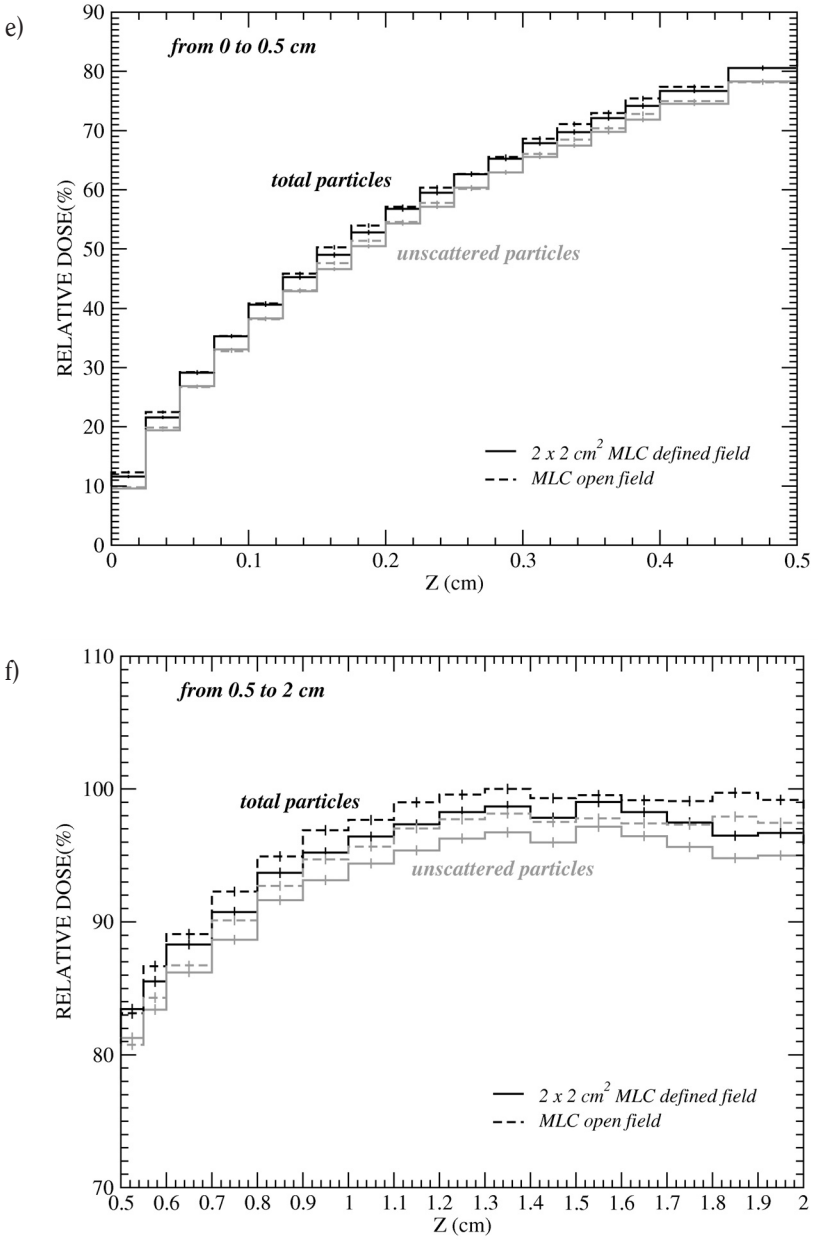

Figure 3e-f. Build-up depth dose curves for the MLC defined field size of 2×2 cm² in comparison to the MLC open field respective ones (dashed line). The components of the dose due to unscattered particles are shown (grey line). The curves were normalized to the D_{max} of the total dose curve for the MLC open field

Figure 4a–4b present the dose build-up curves for the asymmetric field (3×7 cm^2), the observed MLC effect is roughly the same we observed for the 4×4 and the 10×10 cm^2 field sizes.

Total head-scattered particles contribution to total dose as function of field size

Figures 3a–3f and 4a–4b present also the relative central-axis depth dose curves calculated for unscattered particles only, for MLC defined fields and MLC open fields.

By comparison of the total dose and the component of the dose due only to unscattered particles we can see the overall effect of the accelerator head on the build-up dose curve.

For the largest field (10×10 cm^2), the contribution from the accelerator head to the total dose is about 10% on the first 7 mm from the surface, and it decreases gradually to about 6% at the depth of dose maximum. As we expected, this contribution decreases with field size, from 4% for 4×4 cm^2 to 2–3% for the field size of 2×2 cm^2. Finally, for the asymmetric field, the overall head accelerator effect is about 4–5% of the total dose.

By comparing the curves for the MLC defined fields and MLC open fields, the behaviour of the MLC effect in the build-up region for the unscattered particles contribution is similar to the one obtained for total dose curves.

Table 1 summarizes the differences between the total dose and the dose due only to unscattered particles near the phantom surface. These surface dose values were calculated directly in the voxel from 0 to 0.025 cm depth. The scattered particles

Table 1. Surface dose calculated in the voxel from 0 to 0.025 cm depth for different MLC defined field sizes, as shown in Figures 3 and 4. Total and unscattered particles contributions are shown. The absolute uncertainty of each value is presented

MLC defined field size	Surface dose (Total dose) [%]	Surface dose (Unscattered particles) [%]
10×10 cm^2	18.88 ± 0.26	9.80 ± 0.10
4×4 cm^2	13.02 ± 0.23	9.65 ± 0.13
2×2 cm^2	11.58 ± 0.26	9.56 ± 0.13
3×7 cm^2	13.68 ± 0.28	9.63 ± 0.13

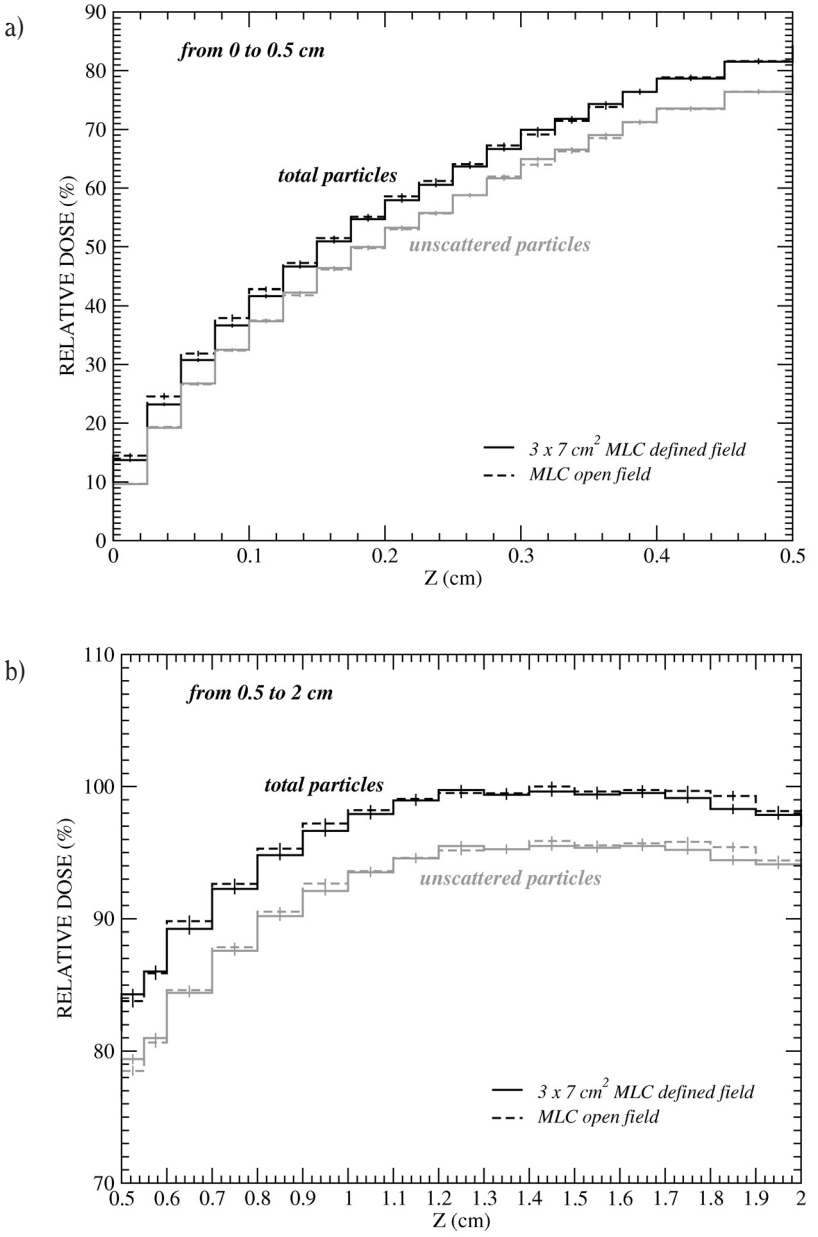

Figure 4a-b. Build-up depth dose curves for MLC defined field size of 3×7 cm^2 in comparison to the MLC open field respective ones (dashed line). The components of the dose due to unscattered particles are shown (grey line). The curves were normalized to the D_{max} of the total dose curve for the MLC open field

component is responsible for the increase of the relative surface dose from about 10% to 19% for the 10×10 cm^2 field. This enhancement effect decreases with field size, being a factor of 4 smaller for the 2×2 cm^2 field compared to 10×10 cm^2 field.

Analysis of fluence spectra at phantom surface

Figures 5a–c present the normalized total fluence of particles and individual contribution of electrons reaching the plane at SSD = 95 cm for the studied MLC symmetric openings. Figures 6a–f show the contribution of particles and electrons scattered from MLC and JAWS to the total fluence. All presented fluence spectra were scored within the field and also 3 cm over the geometric respective edge for each MLC defined field. Several subdivisions are considered according to the last scattering process suffered by electron and particles: from MLC only, from JAWS only and from both JAWS and MLC. For each field, all values are normalized to the maximum value of total particle fluence.

It can be seen that the electrons contribution represent only about 0.15% of the total number of particles reaching the phantom surface for the 10×10 cm^2 MLC defined field and it decreases with field size, from 0.045% for 4×4 cm^2 to 0.025% for the smallest (2×2 cm^2) MLC defined field. The figure also shows that the electron contribution outside the field vary slightly (~20%) with the distance to the beam axis.

In Figures 6b, 6d and 6f, it is observed that about 8%, for 10×10 cm^2, and 3% for smaller fields, of the total electron fluence is due to electrons scattered from JAWS only, from MLC only or from both, JAWS and MLC. There are no significant differences between the JAWS and MLC independent contributions to the total electron fluence.

The fluence of particles at the phantom surface including contributions from JAWS and MLC is also shown in Figures 6a–f. It can be seen that the number of particles scattered from JAWS only represents about 0.2% of the total number reaching the phantom surface for the broad beam (10×10 cm^2) and no significant differences are observed for the contribution from MLC only. Lower contributions are observed as the field size decreases, being 0.05% for 4×4 cm^2 and 0.02% for 2×2 cm^2 MLC defined fields.

The on-axis photon and electron energy spectra are presented in Figures 7 for the 2×2 cm^2 and 10×10 cm^2 MLC defined fields and the respective MLC open fields. The energy bins used for the calculation were 100 keV and 200 keV wide for photons and electrons, respectively. The electron spectra shown in Figures 7b were calculated for a larger region (3×3 cm^2 and 8×8 cm^2 for the smaller and larger field sizes, respectively)

Figure 5. Relative planar fluence as a function of the distance to the beam axis. Only the total distribution and electron contribution were included. The MLC defined field was simulated to get a (a) 10×10 cm^2, (b) 4×4 cm^2 and (c) 2×2 cm^2 at 95 cm SSD. The planar fluence was calculated in the area defined by half-width of (a) 8 cm, (b) 6 cm and (c) 4 cm which was divided in 50, 25 and 15 equal square bins, respectively

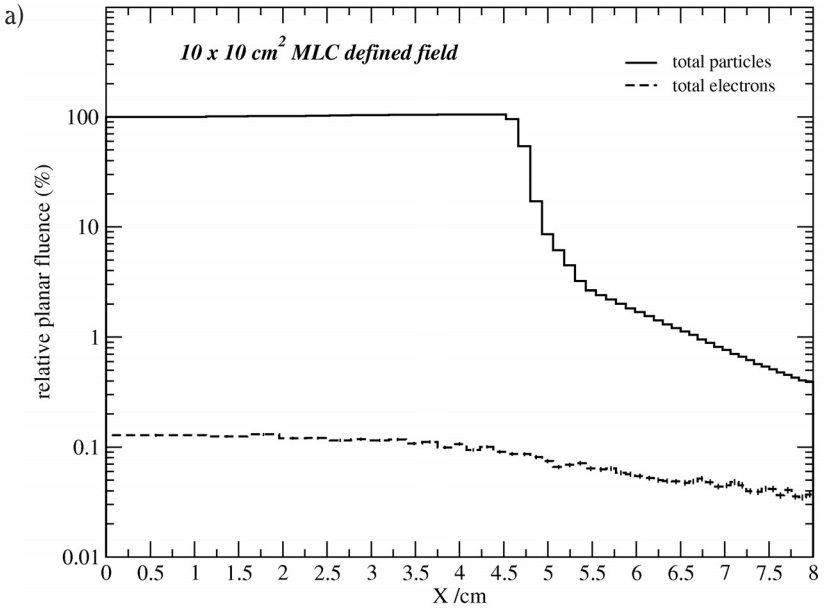

because of the poorer statistics. For the field of 2×2 cm^2 the electron spectra were also calculated for 1×1 cm^2 scoring region and the results were similar because the electrons spread well outside the photon beam. For each field configuration, the spectra were normalized to the maximum value of total particle fluence calculated for the MLC defined field curve.

In relation to total photon fluence, there are not differences between the MLC defined fields and the MLC open fields in the overall spectra. Maximum values in the photon spectra are found around 0.55 MeV and 0.45 MeV for the 2×2 cm^2 and 10×10 cm^2 MLC defined field, respectively. The same values are obtained for the respective MLC open fields.

In Figure 7b it can be seen that the electron fluence for 2×2 cm^2 MLC defined field represents about 0.016% of the total number of particle for the lower energies (< 0.5 MeV). However, this value is about 0.034% for the respective MLC open field. For

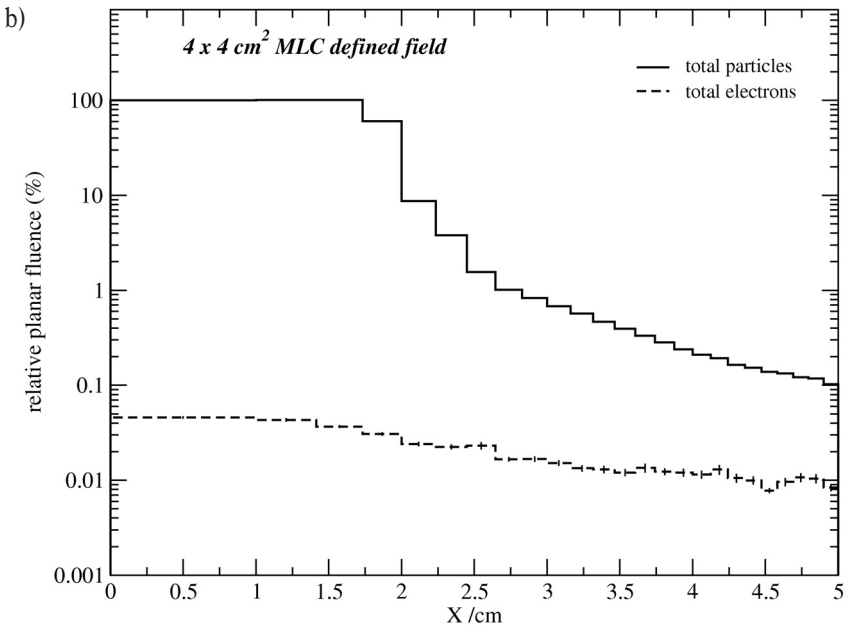

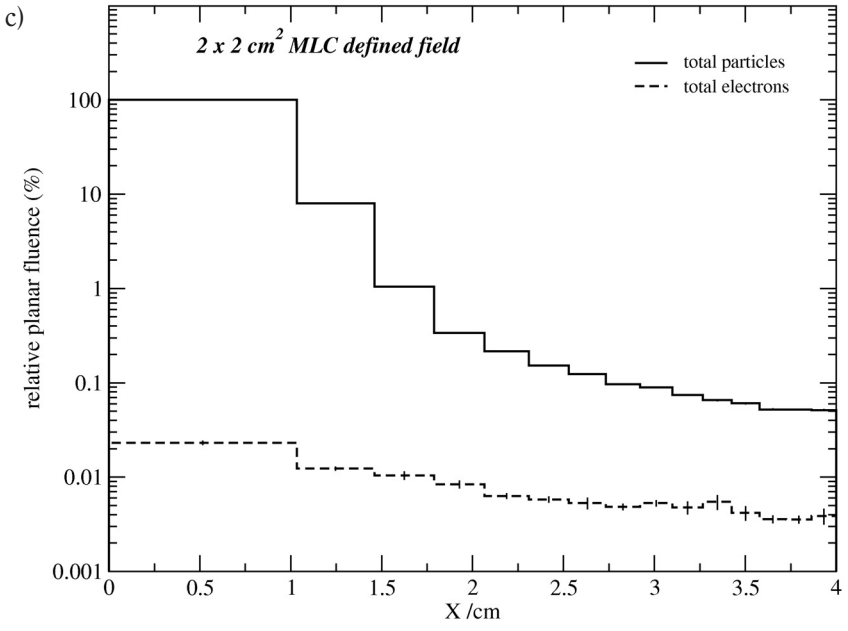

Figure 5b-c

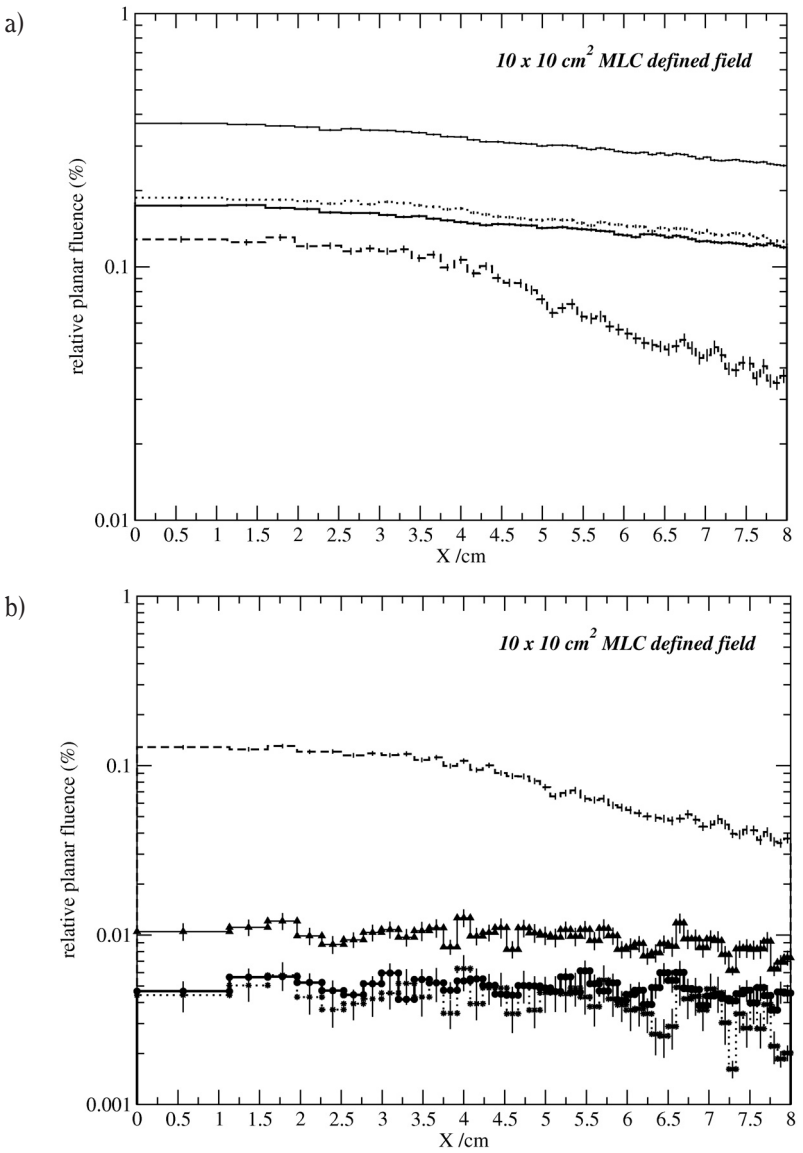

Figure 6a-b. Relative planar fluence as a function of the distance to the beam axis for different MLC defined fields. Total electron contribution (dashed line) and various contributions of particles (top) and electrons (bottom) to the total fluence are represented: particles scattered from MLC only (thick solid line), from JAWS only (dotted line) and from both MLC and JAWS (thin solid line); electrons scattered from MLC only (circles), from JAWS only (stars) and from both MLC and JAWS (triangle up)

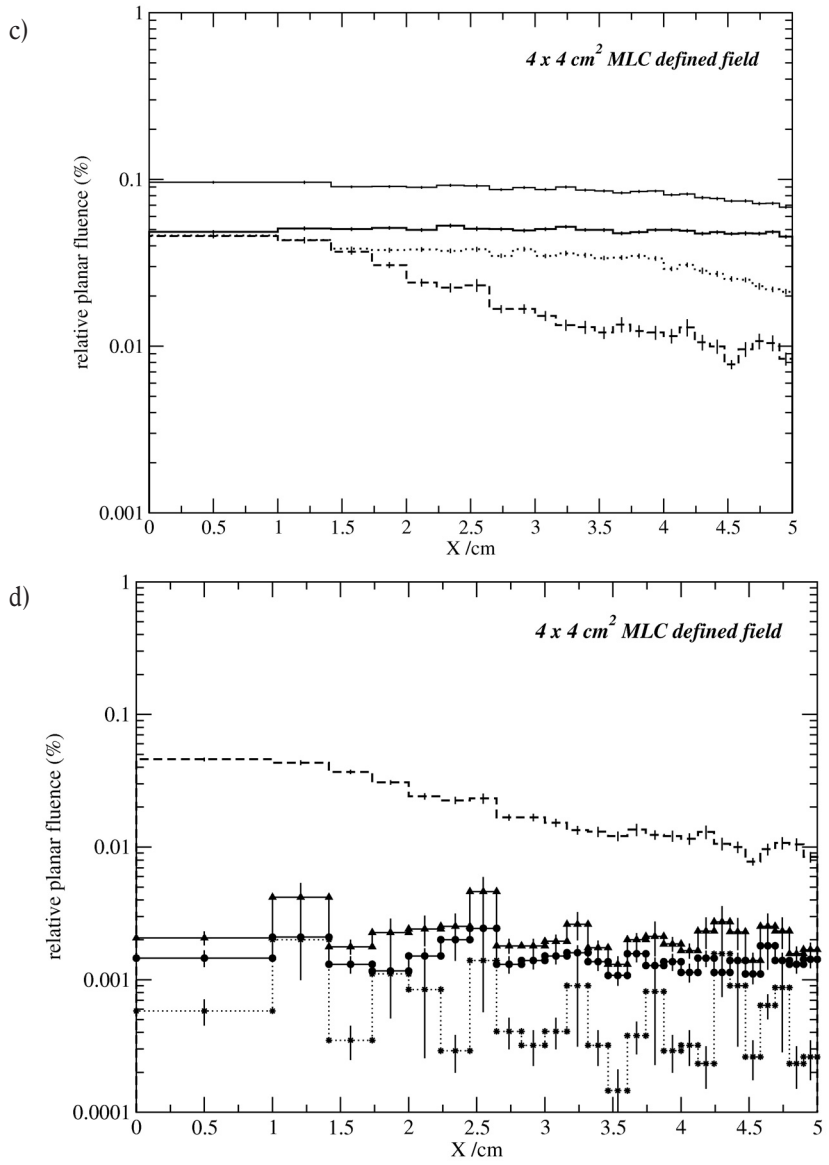

Figure 6c-d. Relative planar fluence as a function of the distance to the beam axis for different MLC defined fields. Total electron contribution (dashed line) and various contributions of particles (top) and electrons (bottom) to the total fluence are represented: particles scattered from MLC only (thick solid line), from JAWS only (dotted line) and from both MLC and JAWS (thin solid line); electrons scattered from MLC only (circles), from JAWS only (stars) and from both MLC and JAWS (triangle up)

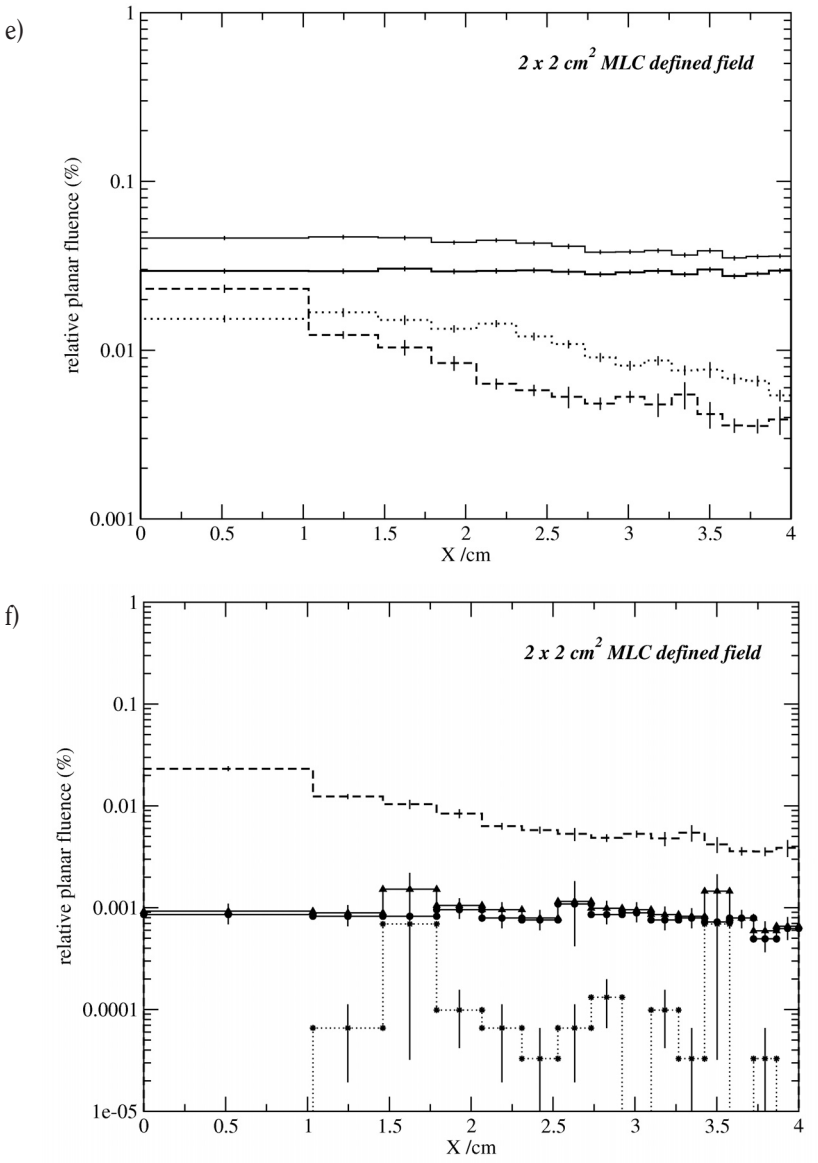

Figure 6e-f. Relative planar fluence as a function of the distance to the beam axis for different MLC defined fields. Total electron contribution (dashed line) and various contributions of particles (top) and electrons (bottom) to the total fluence are represented: particles scattered from MLC only (thick solid line), from JAWS only (dotted line) and from both MLC and JAWS (thin solid line); electrons scattered from MLC only (circles), from JAWS only (stars) and from both MLC and JAWS (triangle up)

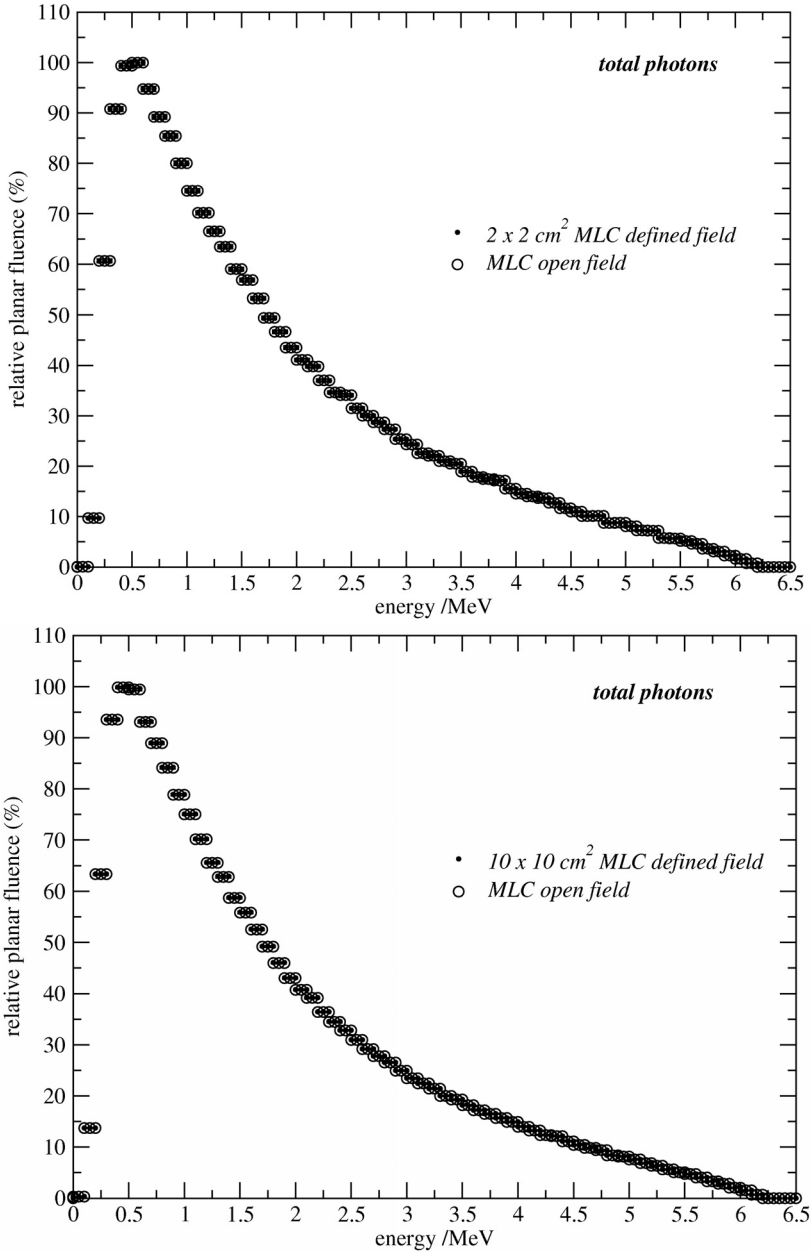

Figure 7a. On-axis energy spectra of photons reaching the scoring plane at 95 cm SSD for 2×2 cm² (top) and 10×10 cm² (bottom) MLC defined fields and the respective MLC open fields. The photon spectra were calculated for scoring regions of 1×1 cm² (top) and 2×2 cm² (bottom). Energy bins were 100 keV wide for photon spectra

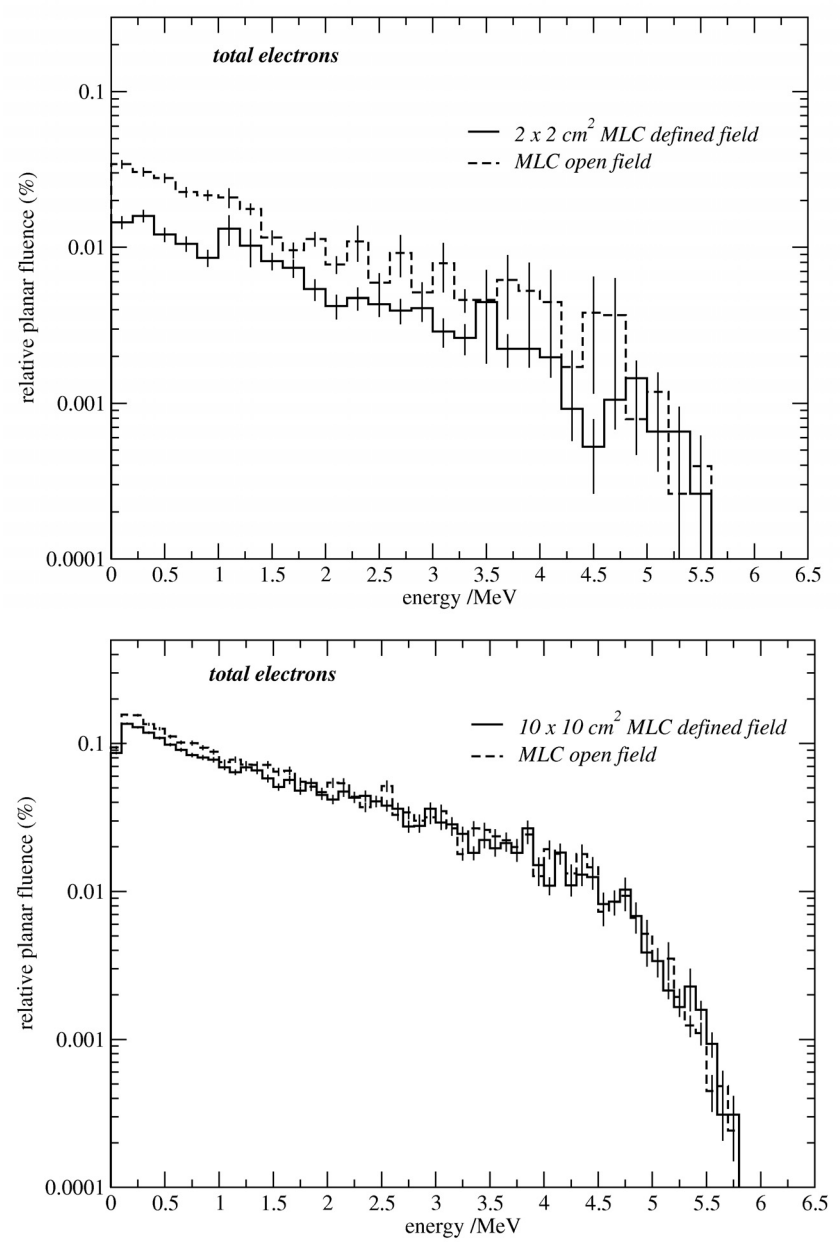

Figure 7b. On-axis energy spectra of electrons reaching the scoring plane at 95 cm SSD for 2×2 cm^2 (top) and 10×10 cm^2 (bottom) MLC defined fields and the respective MLC open fields. The electron spectra were calculated for scoring regions of 3×3 cm^2 (top) and 8×8 cm^2 (bottom). Energy bins were 200 keV for electron spectra

the 10×10 cm^2 MLC defined field the electron fluence is about 10 times higher than those values for 2×2 cm^2 field. For both fields, the electron fluence decreases with the energy. The relative uncertainty of the calculated electron fluence for the 10×10 cm^2 field is about 2% for lower energies (until 1.5 MeV) and it is poorer for the rest of the spectra. For the 2×2 cm^2 case, our calculated values of the electron fluence have relative uncertainty of about 9% for the energy region below 1 MeV. After that, the statistics decreases.

Conclusions

The effect of the MLC on the build-up region dose has been studied using Monte Carlo simulations.

Build-up dose curves for MLC defined fields were compared to fields in which MLC no intercept the beam and the scattering of the MLC does not affect the field. It has been determinate that this effect is practically negligible (less than 1%) for 10×10 and 4×4 cm^2 MLC defined fields. The bigger effect (about 2%) was observed for the 2×2 cm^2 MLC defined field. In the build-up region, the overall head accelerator contribution to the total dose (including MLC) is of about 10% for the 10×10 cm^2 field and it decreases with field size (2–3% for 2×2 cm^2 field size).

The surface dose was calculated directly in the voxel from 0 to 0.025 cm depth of the water phantom for the four fields sizes studied. It was found that the scattering of particles from accelerator head and MLC is responsible for the increase of about 7% on the surface dose by comparing 2×2 and 10×10 cm^2 field sizes.

Acknowledgements

This work was supported by Fundacao para a Ciencia e a Tecnologia grant SFRH/BD/28918/2006.

References

[1] Heath E, Seuntjens J. Development and validation of a BEAMnrc component module for accurate Monte Carlo modelling of the Varian dynamic Millenium multileaf collimator. Phys Med Biol. 2003; 48: 4045–4063.

[2] Jang SY, Vassiliev ON, Liu HH, Mohan R, Siebers JV. Development and commissioning of a multileaf collimator model in Monte Carlo dose calculations for intensity-modulated radiation therapy. Med Phys. 2006; 33(3): 770–781.

[3] Kim JO, Siebers JV, Keall PJ, Arnfield MR, Mohan R. A Monte Carlo study of radiation transport through multileaf collimators. Med Phys. 2001; 28: 2497–2506.

[4] Mora GM, Maio A, Rogers DWO. Monte Carlo Simulation of a Typical ^{60}Co Therapy Source. Med Phys. 1999; 26: 2494–2502.

[5] Rogers DWO, Walters B, Kawrakow I. BEAMnrc Users Manual. Ottawa: National Research Council of Canada; 2005. Report PIRS-0509(A)revK.

[6] Walters B, Kawrakow I, Rogers DWO. DOSXYZnrc Users Manual. Ottawa: National Research Council of Canada; 2005. Report PIRS-794revB.